Immature olfactory sensory neurons provide complementary input in the healthy olfactory system

Jordan D. Gregory[1,2], Ryan S. Herzog[1,2], Kendall A. Curtis[1], Michael I. Marar[1] and Claire E.J. Cheetham[1]

1. Department of Neurobiology, University of Pittsburgh School of Medicine, Pittsburgh PA 15213
2. Center for Neuroscience at the University of Pittsburgh, Pittsburgh, PA 15213

Running title: Immature OSN silencing impairs olfaction

Abstract

Adult neurogenesis of olfactory sensory neurons (OSNs) in the rodent olfactory system provides the unique opportunity to understand how new neurons functionally integrate into existing circuitry and contribute to behaviors. Immature OSNs express odorant receptors (ORs), form dendritic knobs with short cilia, and project their axons into the olfactory bulb (OB) where they form functional synapses. Furthermore, immature OSNs respond selectively to odorants and exhibit graded responses in a higher concentration range than mature OSNs, suggesting that they provide a distinct odor input stream. Finally, in mice that lack mature OSNs, sensory input from immature OSNs is sufficient to mediate odor detection and discrimination behavior. What remains unknown, however, is how these immature OSNs contribute to odor-guided behavior in the healthy, intact olfactory system. Here we show, using male and female mice, that chemogenetically silencing immature OSNs impairs odor detection ability without affecting their odor discrimination ability. Furthermore, immature OSN silencing reduces the amplitude of odor-evoked dendritic calcium responses in OB neurons *in vivo*. Together, these findings suggest that immature OSNs provide distinct odor input that complements mature OSN input to contribute to odor-guided behaviors in the healthy, intact olfactory system.

Introduction

Most mammalian neurons are generated embryonically or early in postnatal development and cannot be replaced. In contrast, newborn olfactory sensory neurons (OSNs) are generated from basal stem cells in the olfactory epithelium (OE) throughout life[1,2]. Globose basal cells generate neuronally committed intermediate cells that undergo a developmental program to produce mature OSNs[3–7]. One to two days after terminal cell division, nascent OSNs transition to immature OSNs marked by the expression of both GAP43 and Gγ8[4,5,8–11]. Seven to eight days after terminal division, OSNs downregulate their expression of GAP43 and Gγ8 and upregulate expression of olfactory marker protein (OMP)[1,2,12–14].

Mature OSNs typically express one of ~1,100 odorant receptor (OR) genes[15,16], with mature OSN axons expressing the same OR converging into the same glomeruli in the olfactory bulb (OB)[17–19]. Here, they form synaptic connections with OB neurons, generating a highly organized odor input map. As existing OSNs undergo apoptosis, newborn OSNs are generated concurrently. This constant turnover creates a highly plastic environment in which newborn OSNs must integrate into pre-existing circuitry to contribute to olfaction. Given that OSNs are also generated throughout life in humans, it is important to understand how ongoing OSN neurogenesis contributes to odor processing, plasticity, and odor-guided behavior.

It has been assumed that mature OSNs provide the sole source of odor input to the OB. However, mounting evidence suggests that immature OSNs also contribute to olfaction. OSNs begin to express odorant receptors (ORs) four days after terminal cell division[10], well before the onset of OMP expression. Furthermore, immature OSNs strongly upregulate neurite outgrowth genes[7] and late-stage immature OSNs both project axons into glomeruli in the OB and form dendritic knobs with short cilia[20–24]. Moreover, immature OSNs can detect odorants and form synaptic connections with OB projection neurons in mice[21,23]. Importantly, odor selectivity is similar for immature and mature OSNs[23]. However, compared to mature OSNs, immature OSNs have higher thresholds for odorant detection but continue to encode concentration information at high odorant concentrations at which mature OSN responses are saturated[23]. Furthermore, sensory input from immature OSNs is sufficient to mediate odor detection and discrimination at early recovery time points in mice that have undergone methimazole-mediated OSN ablation[23,25,26]. Together, these data suggest that immature OSNs provide behaviorally relevant information to the olfactory system.

What remains unknown is what contribution, if any, immature OSNs make in the healthy, intact olfactory system. We hypothesize that immature and mature OSNs provide complementary, but

56 distinct, odor input to OB neurons. Here, we used selective chemogenetic silencing[27–29] of immature
57 OSNs to address two key questions. First, do immature OSNs contribute to odor-guided behaviors in
58 healthy mice? Second, do immature OSNs provide odor input to the OB that cannot be supplied by
59 mature OSNs? Silencing immature OSNs impairs odor detection ability but does not affect odor
60 discrimination. Furthermore, acutely silencing immature OSNs reduces the amplitude of odorant-
61 evoked responses in OB neurons *in vivo*. Together, our data suggest that immature and mature OSNs
62 provide complementary odor input to the OB that contributes to distinct aspects of odor-guided
63 behavior.

64 **Results**

65 Selective expression of hM4Di silences ~60% of immature OSNs

66 To determine the contribution of immature OSNs to olfaction in the healthy, intact olfactory system, we
67 bred Gγ8-tTA;tetO-hM4Di (referred to hereafter as Gγ8-hM4Di) and tetO-hM4Di mice. In Gγ8-hM4Di
68 mice, immature OSNs express hM4Di, which silences activity in the presence of a ligand such as
69 clozapine-N-oxide (CNO), specifically in immature OSNs due to tetracycline transactivator (tTA)
70 expression under control of the Gγ8 promoter[27,30] (Fig. 1A). We validated the specificity of hM4Di
71 expression in immature OSNs via co-immunostaining for GAP43 to mark immature OSNs[5] and the
72 hemagglutinin (HA) tag attached to the hM4Di receptor (https://www.jax.org/strain/024114) (Fig. 1B).
73 tetO-hM4Di mice were included as negative controls throughout this study and did not express the
74 hM4Di receptor marked by HA staining (Fig. 1C). Approximately 60% of immature OSNs expressed
75 the hM4Di receptor in Gγ8-hM4Di mice, whereas tetO-hM4Di controls, which lack tTA expression, did
76 not express hM4Di (Fig. 1D).

77 Silencing immature OSNs reduces mitral cell activity in response to odors throughout the OB

78 We first sought to validate our model to acutely silence immature OSNs and determine the effects of
79 immature OSN silencing on odor-evoked mitral cell (MC) activity. We stained the OB for the
80 immediate early gene phospho-S6 (PS6) in saline- and CNO-treated mice after a 1-hour odor
81 exposure session (Fig. 1E,F). We then calculated the linear density of PS6+ cells in the mitral cell
82 layer (MCL) for each mouse. This showed that silencing immature OSNs significantly decreased the
83 density of PS6-expressing MCs, indicating that MC activity was reduced as a result of immature OSN
84 silencing (Fig. 1G; saline-treated Gγ8-hM4Di n = 4, CNO-treated Gγ8-hM4Di n = 4). Recent evidence
85 has shown that the ventral OE contains a larger proportion of immature OSNs than the dorsal OE[31].
86 Given the topography of OE-OB projections, this led us to ask whether MC activity in the dorsal vs.
87 ventral OB is differentially affected by immature OSN silencing. Subdividing the MCL showed that

immature OSN silencing had a significant effect on MC activity in both dorsal and ventral regions (Fig. 1H,I). This reduction in MC PS6 staining was not present in CNO-treated tetO-hM4Di control mice (Fig. 1J-L), thus validating our strategy to acutely and selectively silence immature OSN input throughout the OB.

Immature OSN silencing impairs odor detection behavior

Odor detection ability was tested using a buried food assay wherein mice are given 10 minutes to complete the task. In Gγ8-hM4Di mice, all saline-injected mice successfully uncovered the buried food within the 10-minute period (n = 7 mice), whereas 2/8 CNO-injected Gγ8-hM4Di mice failed to uncover the buried food (Fig. 2A). The time taken to uncover the buried food was significantly longer for CNO-treated than for saline-treated Gγ8-hM4Di mice (Fig. 2A). There was no effect of CNO treatment on the time spent digging during the five-minute acclimation period for Gγ8-hM4Di mice (Fig. 2B). In tetO-hM4Di control mice, 3/5 saline-injected and 2/3 CNO-injected mice uncovered the buried food. There was no difference in the time to complete the task between saline- (n=5) and CNO-treated (n=5) tetO-hM4Di mice (Fig. 2C). There was also no difference in acclimation period digging time between saline- and CNO-treated tetO-hM4Di mice (Fig. 2D). Together, these data show that odor detection ability is impaired when immature OSNs are silenced.

Immature OSN silencing does not affect odor discrimination in a habituation-dishabituation task

To test whether odor discrimination ability is impacted by silencing immature OSNs, we performed an odor habituation-dishabituation task using Gγ8-hM4Di mice[23] (Fig. 2E). We found no effect of immature OSN silencing via CNO administration on total investigation time (Fig. 2F), habituation index (Fig. 2G) or dishabituation index (Fig. 2H). We also found no effect of CNO administration on odor habituation-dishabituation in tetO-hM4Di control mice (Fig. 2I); total investigation time (Fig. 2J), habituation index (Fig. 2K) and dishabituation index (Fig. 2L) were unaffected. These data suggest that silencing immature OSNs does not impact odor discrimination ability in this task.

Immature OSN silencing reduces the amplitude of odor-evoked responses in the GL of the dorsal OB

To investigate the impact of immature OSN silencing on odor-evoked responses in OB neurons, we implanted acute cranial windows over the right OB of 3-5-week-old Gγ8-hM4Di and tetO-hM4Di mice that had received a neonatal injection of AAV5-syn-GCaMP6s directly into the right OB (Fig. 3A & B). This allowed us to record odor-evoked responses in the glomerular layer (GL) of the olfactory bulb *in vivo* before and after CNO injection. Neonatal AAV5-syn-GCaMP6s injection resulted in GCaMP6s expression in neuronal types throughout the OB (Fig. 3C & D), but most prominently in the MCL, external plexiform layer (EPL), and the GL of the OB. Linear density analysis of GCaMP6s-expressing

cells in these OB layers revealed that a majority of the cells were found in the MCL (Fig. 3E) with apical dendrites of putative MCs and tufted cells (TCs) expressing GCaMP6s also projecting into the GL. Thus, MC and TC dendrites are likely to be a major contributor to the GL odor-evoked calcium responses that we report using AAV5-syn-GCaMP6s.

We found that silencing immature OSNs significantly reduces the amplitude of odor-evoked glomerular responses across a panel of seven odorants (Fig. 3F, Videos S1 & S2). Our findings in Fig. 3F are reported as mean odor-evoked responses for each imaged mouse. When we analyzed the individual glomeruli that contribute to these per mouse mean responses, we saw a similar decrease in the amplitude of odor-evoked responses after CNO treatment (Fig. S1A). Hence, immature OSNs make a meaningful contribution to the odor information that is supplied to the OB in healthy adolescent mice. To further evaluate the odor selectivity of these responses before and after immature OSN silencing, we calculated the lifetime sparseness (S_L) of glomerular odorant responses. An S_L value of 1 indicates that a glomerulus responds to a single odorant (highly selective), whereas an S_L value of 0 indicates that a glomerulus responds equally to all seven odorants in our panel (non-selective). We found that odor selectivity is not impacted by immature OSN silencing (Fig. 3G). CNO administration in tetO-hM4Di control mice did not impact the amplitude of odor-evoked responses *in vivo* (Fig. 3H, Fig. S1B) and did not affect odor selectivity (Fig. 3I). Together, these results suggest that immature OSNs contribute to the odor input received by OB neurons in the healthy, intact olfactory system.

Discussion

In this study we sought to define the contribution of immature OSNs to olfaction in the healthy, intact olfactory system. We showed that chemogenetically silencing immature OSNs in awake, behaving mice impairs odor detection ability without hindering odor discrimination in a habituation-dishabituation assay. Furthermore, silencing immature OSNs results in decreased neuronal activity marked by immediate early gene expression in MCs throughout the OB and a broad reduction in the amplitude of odor-evoked responses across multiple glomeruli *in vivo* without affecting odor selectivity. Together, these data suggest that immature OSNs provide complementary odor input to that supplied by mature OSNs in the intact olfactory system. Hence, our findings provide further evidence that endogenously generated postnatally born neurons, once integrated into the existing circuitry, provide functional information for odor processing.

An important question to address is what proportion of sensory input to the OB is being silenced by CNO treatment in Gγ8-hM4Di mice. Our approach to express the inhibitory DREADD hM4Di utilized a

tetracycline operator (tetO) sequence activated by expression of tetracycline transactivator (tTA) in immature OSNs under control of the Gγ8 promoter. Validation of our model revealed that approximately 60% of GAP43+ (i.e. immature) OSNs express hM4Di, as marked by hemagglutinin (HA) tag expression (Fig. 1B-D). Data from a previous study[21] that assessed linear densities of immature and mature OSNs in the OE shows that Gγ8+ OSNs make up approximately 29% of the OSN population in 8-week-old mice (this value excludes nascent OSNs as they do not provide sensory input to the OB). Additionally, immature OSNs express GAP43 and Gγ8 from 1-7 days after terminal cell division[5,9,14], which defines the population of immature OSNs in which hM4Di is expressed. However, immature OSNs do not project to the OB until 5 to 7 days after terminal cell division[4,23]. This limited window of both Gγ8 expression (which drives hM4Di expression in only 60% of immature OSNs) and the 2-3 day timeframe during which immature OSNs project to the OB before reaching maturity as defined by OMP expression (a fraction of 3/7 of Gγ8-expressing OSNs, assuming a uniform neurogenesis rate) results in an estimate that we are silencing a maximum of 12% of OSNs projecting to the OB at a given time (Gγ8+ account for 29% of all OSNs and 3/7 of these project to the OB = 12%). To that end, reducing OSN input into the OB seems to have surprisingly significant effects on olfactory-guided behaviors and odor-evoked responses, suggesting that their input may be distinct from that provided by mature OSNs.

We have shown previously that a subset of mice can perform odor detection and discrimination tasks, including the tasks used in the current study, using only immature OSNs following methimazole-mediated OSN ablation and subsequent regeneration of OSNs[23]. In that previous study, early recovery timepoints at which mature OSNs are absent from the olfactory epithelium were tested[23]. However, an important remaining question was whether immature OSN activity is necessary for odor-guided behaviors in the healthy olfactory system. Here, we demonstrated that silencing immature OSNs impairs odor detection ability in the buried food task (Fig. 2A) without affecting odor discrimination ability in an olfactory habituation-dishabituation task (Fig. 2E-H). This suggests that immature OSN input may be less important for odor discrimination behavior, although additional assays should be performed to strengthen this conclusion. Why do immature OSNs play a particularly important role in buried food detection? Our previous finding that immature OSNs encode odor concentration information high in the concentration range, when mature OSN responses have already saturated[23], provides a potential explanation: immature OSNs may play an important role in odor source localization. Hence, sensory input from mature OSNs may play a more important role far from the buried food, whereas immature OSN input is important, or even necessary, to pinpoint the exact location.

How can we reconcile the seemingly conflicting findings that immature OSNs can mediate odor discrimination, yet immature OSN silencing in the intact olfactory system does not impair odor discrimination, using the same task? A simple explanation is that immature OSNs, if present in adequate numbers, are sufficient for odor discrimination, but they are not necessary for odor discrimination in the intact olfactory system, in which large numbers of mature OSNs are also present. We have estimated an upper limit of 12% of total OSN input being silenced in CNO-treated Gγ8-hM4Di mice. Hence, if immature OSNs do not play a distinct role in odor discrimination, the relatively small reduction in total OSN input in CNO-treated Gγ8-hM4Di mice is unlikely to reduce success rate in this simple odor discrimination task. Our calcium imaging data showed that silencing immature OSNs reduces the amplitude of odor-evoked responses in postsynaptic OB neurons *in vivo*. Our AAV5-based strategy to introduce GCaMP6s into OB neurons does result in expression throughout all layers of the OB, but GCaMP6s is preferentially expressed in the MCL and EPL of the OB (Fig. 3C-E). Thus, we reason that MC and TC dendritic responses are a major contributor to the GL GCaMP6s responses that we imaged. A similar effect of immature OSN silencing on GCaMP6s responses was seen across our odor panel, which includes the major odorant functional groups of esters (ethyl butyrate, isoamyl acetate, ethyl valerate, methyl valerate, and methyl butyrate), an aldehyde (hexanal), and an amine (phenethylamine) (Figs. 3F, S1A; Videos S1 & S2). Additionally, we sampled from a random population of glomeruli across the dorsal surface of the OB in each mouse. These factors together suggest that the reduction in odor-evoked response amplitude elicited by immature OSN silencing is a generalized phenomenon in glomeruli populating at least the dorsal surface of the OB. This suggests that immature OSNs that project to the OB GL contribute to ongoing odor processing in the healthy olfactory system.

We also found that immature OSN silencing did not affect the odor selectivity of odor-evoked responses in OB neurons (Fig. 3G). This finding agrees with our previous study, which found that the selectivity of odor-evoked responses was similar in immature and mature OSN axons[23]. In contrast, single cell RNA sequencing studies found that some immature OSNs express multiple OR transcripts[32,33], which might be expected to reduce odor selectivity. The explanation for this discrepancy is provided by a recent study describing a Mex3a-dependent post-transcriptional regulatory mechanism that represses translation of multiple ORs in immature OSNs[34].

A limitation of this study is that imaging was restricted to dorsal OB glomeruli, due to their optical accessibility. Hence, while silencing immature OSNs reduces the amplitude of dorsal GL odor-evoked responses, does silencing have a similar impact in other OB regions? Furthermore, mice were sedated using dexmedetomidine for imaging. While the half-life for dexmedetomidine elimination has

not been measured in mice, it is ~65 min in rats[35], suggesting that sedation depth would be gradually decreasing during the ~90 min time course of our imaging experiments. Given that odor representations are sparser in awake than in anesthetized mice[36,37], changes in sedation depth could have affected the amplitude of odor-evoked responses over time.

Our immediate early gene staining of odor-evoked MC activity shows a significant reduction in the number of PS6 positive cells throughout the OB (Fig. 1G). We also found that immature OSN silencing had a similar effect on MC activity in the dorsal and ventral halves of the OB (Fig. 1H,I). This was surprising in light of a recent study showing that ventral OE regions have a greater proportion of immature OSNs than dorsal OE regions[31], which might be expected to result in greater immature OSN innervation of ventral vs. dorsal OB. While more sensitive assays of neuronal activity, that also assess other OB neuron types, might detect such a difference, the key finding here is that immature OSN input is sufficient throughout the OB to impact MC activity when it is silenced.

Together, our data highlight the important contribution of postnatally born OSNs to normal odor processing even while these cells are in development. It was once believed that newborn OSNs did not functionally contribute to olfactory circuity until they had reached maturity. In contrast, we have shown that immature OSNs not only make up a contribution to odor-evoked responses but also provide odor input that is useful in performed odor-guided behaviors, and cannot be supplied by mature OSNs, in the healthy olfactory system. Hence, we reason that immature OSNs provide complementary input to that supplied by mature OSNs that is essential for olfactory processing and odor-guided behaviors that are important for survival.

Methods

Experimental animals

All animal procedures conformed to the National Institute of Health guidelines and were approved by the University of Pittsburgh Institutional Animal Care and Use Committee. Mice were housed on a 12-hour light/dark cycle in individually ventilated cages at 22°C and 48% humidity with unrestricted access to food and water unless otherwise stated. Mice were group-housed if same sex littermates were available. A total of 59 mice was used in this study.

Generation of the Gγ8-tTA[30] and tetO-hM4Di[27] (Jackson Laboratory strain #024114) mouse lines has been published. Separate cohorts of experimental mice were used for the following: behavioral testing (buried food and habituation/dishabituation tests) (age range: 6 to 8 weeks), *in vivo* 2-photon calcium imaging (age range: postnatal days 24 to 35 [P24-35]) and immunohistochemistry (age range: 6 to 8 weeks). All mice used were either Gγ8-hM4Di [Gγ8-tTA$^{+/-}$;tetO-hM4Di$^{+/-}$] or tetO-hM4Di$^{+/-}$

genotypes. Each experimental group comprised roughly equal numbers of male and female mice. Mice of each genotype were randomly assigned to each experimental group for behavioral testing. Mice were genotyped by PCR using previously validated primers as described previously[23] (https://www.jax.org/Protocol?stockNumber=024114&protocolID=26393).

Clozapine-N-Oxide (CNO) treatment to silence immature OSNs

30 minutes prior to starting behavioral or 2-photon calcium imaging experiments (to allow for CNO to begin taking effect), mice received a single intraperitoneal injection of either saline (vehicle) or CNO (1 mg/kg; 10 µl/g). All experiments were conducted 30 minutes after injection to allow for the CNO to have taken effect well but remain within its ~1-hour half-life[38,39].

Odor exposure assay for immediate early gene phospho-S6 immunohistochemistry

30 minutes prior to odor exposure, mice (age range: 6 to 8 weeks) received an i.p. injection of either CNO or saline and were housed in a separate empty home cage to allow the drug to take effect. After these 30 minutes passed, mice were then placed individually into new empty home cages with the cage lid on and were exposed for 1 hour to a glass vial with a perforated lid containing a mixture composed of 30 µL each of the following odorants diluted 1:10 in mineral oil: isoamyl acetate, ethyl butyrate, methyl valerate, and isovaleric acid. Mice underwent transcardial perfusion immediately after the 1-hour exposure.

Transcardial perfusion and cryosectioning

Mice were deeply anesthetized using 4% isoflurane in 1L/min O_2 and transcardially perfused with phosphate buffered saline (PBS) followed by 4% paraformaldehyde (PFA). The OBs of these mice were then dissected out, cryoprotected in a 30% sucrose solution, embedded in 10% gelatin, fixed/cryopreserved, flash frozen, and sectioned on a cryostat for immunostaining as described previously[23].

Immunohistochemistry in OB and OE sections

Free floating OB and OE sections were treated with 1% sodium borohydride, washed with PBS, and then permeabilized for one hour in blocking buffer (5% normal donkey serum [NDS]/0.5% Triton X-100 in PBS). 40 µm OB sections were then stained with a primary antibody to detect the immediate early gene (IEG) phospho-S6 (PS6). 40 µm OB sections from mice that had been neonatally injected with AAV5-syn-GCaMP6s were stained with anti-GFP-ATTO488 nanobody. 50 µm OE sections were co-stained with primary antibodies to detect immature OSNs via growth-associated protein 43 (GAP43) and the hM4Di receptor via its hemagglutinin (HA) tag. All sections were incubated in

primary antibody solutions (3% NDS, 0.2% Triton X-100, 0.01% sodium azide in PBS) as shown in Table 1. Following primary antibody application, sections were washed in PBS and then incubated in secondary antibody solution (3% NDS, 0.2% Triton X-100 in PBS) for one hour at room temperature (except for ATTO-488-GFP staining, which did not require secondary antibody incubation). Sections were then washed in PBS and mounted with Vectashield containing DAPI (Vector Labs).

Antibody	**Dilution**	**Species**	**Incubation conditions**	**RRID**	**Manufacturer catalog #**
GAP43	1:500	Mouse	96 h | 4 °C	AB 2533123	ThermoFisher 33-5000
Anti-HA	1:250	Rabbit	96 h | 4 °C	AB 1549585	Cell Signaling Technology #3724
Phospho-S6	1:400	Rabbit	96 h | 4 °C	AB 916156	Cell Signaling Technology #4858
ATTO-488-GFP	1:500	Camelid	1 h | room temp.	AB_2631386	Chromotek #gba488
Rabbit-AF488	1:500	Donkey	1 h | room temp.	AB 2535792	ThermoFisher A21206
Rabbit-AF 546	1:500	Donkey	1 h | room temp.	AB 2534016	ThermoFisher A10040
MouseAF-546	1:500	Donkey	1 h | room temp.	AB 11180613	ThermoFisher A10036

Table 1: Primary and secondary antibody information

Confocal microscopy

Images of stained OE sections were acquired using an Olympus Fluoview 3000 confocal microscope with an Apo 60x/1.4 NA oil-immersion objective and Fluoview imaging software (Olympus). Laser excitation and bandpass emission filters were: 405 nm and 450/50 for DAPI, 488 nm and 525/50 for AF488, and 561 nm and 595/50 for AF546. Z series images were collected with 2 µm steps between each z plane. Images were 212.1 x 212.1 µm (1024 x 1024 pixels) collected with a 2.0 µs/pixel sampling speed.

Widefield fluorescence microscopy

Images of OB sections were collected using Echo imaging software (Discover Echo) on a Revolve microscope equipped with LED excitation (Discover Echo) and a Plan Apo 10x/0.4 NA air objective (Olympus). Images were stitched together in Affinity Photo software (Affinity). Bandpass emission filter wavelengths were (in nm): DAPI (450/50), GFP (495/50) and Phospho-S6-AF546 (590/50). Detection settings were identical for all images collected for this dataset.

Image analysis in OB and OE sections

Image analysis for PS6 intensity in OB sections, colocalization of GAP43 and HA in OE sections and GCaMP6s expression in OB sections was performed in Fiji (ImageJ)[40]. Images of OB sections were subdivided into dorsal and ventral halves by horizontally bisecting the image halfway along a vertical line extending from the center of the dorsal surface to the center of the ventral surface. MCs, defined as large neurons within the MCL, that expressed PS6 were counted and the length of the MCL/EPL border was measured, for dorsal and ventral halves of each section. PS6+ MC linear density (MCs per mm) was then calculated separately for each half, and as a total value for the entire section. Cells expressing GCaMP6s (as marked by anti-GFP staining) were counted in the MCL, EPL and GL, and their density in each layer was calculated. OSNs expressing either GAP43 or HA were marked separately in z-stacks, and the proportion of immature OSNs in the OE that expressed the hM4Di receptor was calculated by dividing the number of co-stained (GAP43+ and HA+) cells by the total number of immature (GAP43+) OSNs and converting it to a percentage.

Odor detection and discrimination assays and analysis

A buried food assay[23,41] was used to test odor detection ability following either CNO or saline injection. Two days before testing, a Froot Loop (Kellogg's) was placed into the home cage to familiarize the mice with the target odor. 14 hours prior to testing, mice were placed in a new home cage and food restricted until testing. During testing, 6-8-week-old mice were placed in an empty cage (L: 29.21 cm x W: 19.05 cm x H: 12.7 cm) with 1.5 cm of autoclaved bedding for five minutes to acclimate to the environment. Mice were then removed so that the Froot Loop could be buried in the center of the cage. The mice were then placed back into the cage and given 10 minutes to complete the task. Their behavior during both the acclimation and testing periods was monitored via video recording software (pylon Viewer, Basler). The amount of time spent digging in each 10-minute test session was recorded for each mouse. The time that it took for the mouse to uncover the buried food was reported. Mice failed the task if they did not uncover the buried food within 10 minutes. If mice failed to complete the task within the allotted ten minutes, they were removed from the cage, assigned a time of 10 minutes, and given the cereal to eat in their home cage. Mice that uncovered the buried food

within the allotted 10 minutes of the test were allowed to eat the cereal before being returned to their home cage.

An odor habituation-dishabituation assay was used to test odor discrimination ability in saline or CNO-injected mice, using some modifications from previous protocols[23,41]. Mice were acclimated for 30 minutes to the test cage, which was an empty cage (length: 30.48 cm x width: 19.05 cm x height: 12.7 cm) with a metal tea ball secured to the center of the cage floor. Mice were then presented with a series of odorant-soaked filter paper squares placed in the tea ball for two minutes each. The series of odorants consisted of three 2-minute trials each of water, almond extract, mint extract, and vanilla extract (all diluted 1:100 in water). Live recordings were captured via Pylon viewer software, and investigation of the tea ball during each odor presentation was analyzed using EthoVision tracking software (Noldus). Time spent investigating the tea ball for each odor and total investigation time across the entire test period were calculated. A habituation index value was calculated by subtracting the amount of time the mouse spent sniffing during the second trial from the first trial of each odorant. A dishabituation index value was calculated by subtracting the amount of time the mouse spent sniffing the third presentation of an odorant from the amount of time they spent sniffing the first presentation of the subsequent odorant.

Neonatal AAV injections in mouse olfactory bulbs

At P2, Gγ8-hM4Di and tetO-hM4Di mice were anesthetized by acute hypothermia[42] until immobile and 1 ul of AAV5-syn-GCaMP6s (Addgene #100843-AAV5) was injected into the right OB via a glass micropipette[43]. Mice then recovered on a heating pad until awake and mobile in a separate holding container before being returned to their home cage until they reached imaging age (P24-P35).

Acute window preparation for *in vivo* 2-photon calcium imaging

P24-P35 Gγ8-hM4Di mice were anesthetized with isoflurane (1.5 - 2% in 1L/min oxygen), administered ketoprofen (5 mg/kg) as an analgesic, and received a ~1 mm diameter craniotomy over the right OB where a glass coverslip cranial window was implanted[44] (Fig. 3A & B). A head bar was also attached to the skull between the coronal and lambdoid sutures.

In vivo 2 photon calcium imaging and analysis

After acute cranial window implantation and head bar affixation, mice received dexmedetomidine (0.5 mg/kg; 10 µl/g) for sedation while undergoing imaging. Mice were imaged using ThorImage 4.1 software (ThorLabs) and a Bergamo II 2-photon microscope with a resonant scanner and GaAsP detectors (ThorLabs) using a Semi/Apo 20x/1.0NA water-immersion objective (Olympus), and an

Insight X3 IR laser (Newport) mode-locked at 935 nm to image GCaMP6s fluorescence. An imaging field of view was selected through GCaMP6s expression identified via widefield 490 nm LED (ThorLabs) illumination across the region of the dorsal OB surface visible through the cranial window.

Odorant stimulation was performed using a custom-built Arduino-controlled olfactometer. Stimulation and image acquisition timing were controlled and recorded using Python, ThorSync, and ThorImage (ThorLabs). A panel of seven odorants known to stimulate dorsal surface OB glomeruli was used. The following odorants were used at a 10% concentration diluted in mineral oil (v/v): ethyl butyrate (EB), isoamyl acetate (IAA), hexanal, ethyl valerate (EV), methyl butyrate (MB), methyl valerate (MV), and 2-phenethylamine (PEA). Saturated vapor from odorant vials, or a blank deodorized air control, were delivered via an oxygen carrier stream (1 L/min flow rate). All stimuli were 1 s in duration and were delivered via a tube positioned ~5 mm from the mouse's nose. All image trials were 20 s in duration (3.5 s baseline, 1 s stimulus, 15.5 s post-stimulus). Three trials were collected for each stimulus, with odorants and blank stimuli delivered in a pseudo-randomized order with a 60 s inter-trial interval.

Images were analyzed in Fiji. Glomeruli were manually outlined in each field of view, and these outlines were used for analysis of all stimulus-evoked responses. Fluorescence intensity over time was calculated for each glomerulus for each trial. Mean values from the three trials for each stimulus were then calculated for each glomerulus. Additionally, the mean value across all glomeruli was calculated for each mouse. The fluorescence intensity change (ΔF) was calculated as the difference between a 1 s baseline prior to stimulus onset and peak fluorescence within 3 s after stimulus onset. A glomerulus was defined as responding to a stimulus if the ΔF amplitude was greater than three standard deviations of the baseline period. $\Delta F/F$ (%) was reported as (baseline − peak)/baseline x 100 for significant responses only. For blank subtraction, the $\Delta F/F$ in response to the blank (deodorized air) stimulus for a glomerulus was subtracted from the $\Delta F/F$ in response to each odorant.

Lifetime sparseness (S_L) was calculated to measure the degree of odor selectivity of each glomerulus before and after CNO treatment. S_L was calculated as $(1 - (\Sigma_{i=1,n}(r_i/n)^2)/(\Sigma_{i=1,n}(r_i^2/n)))/(1 - 1/n)$, where r_i is the $\Delta F/F$ of the glomerular response to odorant i and n is the total number of odorants (Huang et al., 2022). A highly odorant-selective glomerulus had an S_L of 1 and a glomerulus that was equally responsive to all odors in the panel had an S_L of 0.

<u>Statistics</u>

Statistical analyses were conducted in Prism 9 or Prism 10 software (GraphPad). All data were tested for normality (Shapiro-Wilk or Kolmogorov-Smirnov test) and equal variance (Browne-Forsyth test) to

determine whether parametric tests could be employed. Co-staining for the HA tag on the hM4Di receptor in immature OSNs (identified via GAP43 expression) in olfactory epithelia of Gγ8-hM4Di and tetO-hM4Di mice was assessed using an unpaired t-test. Linear density of PS6+ cells in saline- vs. CNO-treated Gγ8-hM4Di and tetO-hM4Di mice was compared using unpaired t-tests. For the buried food task, unpaired t-tests were conducted on the time to success and on digging time during the acclimation period. For the habituation/dishabituation task, unpaired t-tests were used to compare total investigation time, habituation index and dishabituation index between saline- and CNO-treated Gγ8-hM4Di and tetO-hM4Di mice. GCaMP6s expression across OB layers was compared using a one-way ANOVA with Tukey's multiple comparisons tests. Odor-evoked calcium responses before and after CNO treatment were analyzed using two-way ANOVAs. Finally, paired t-tests were used to compare lifetime sparseness before and after CNO treatment.

Figures

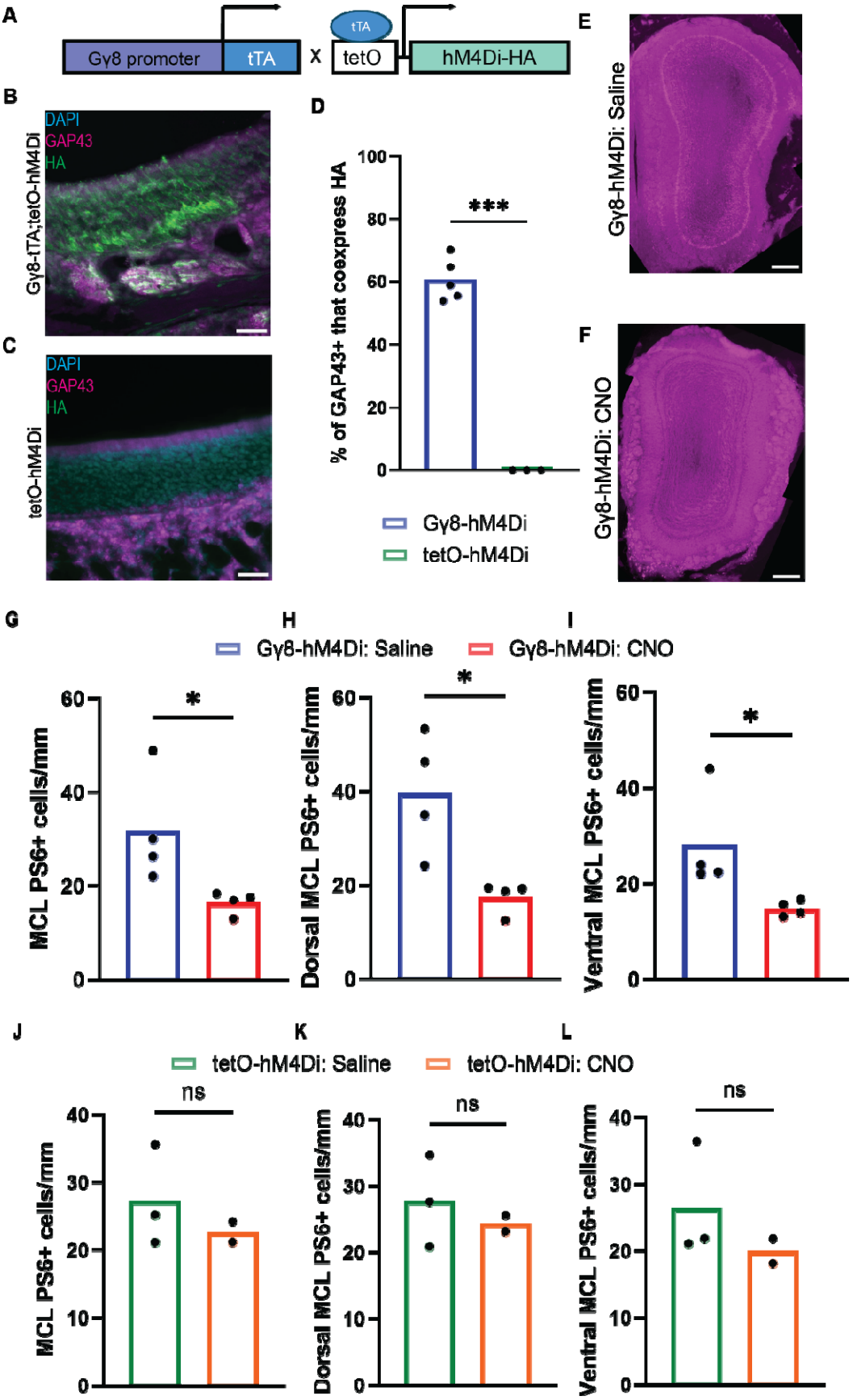

Figure 1. Validation of transgenic approach to silence immature OSNs. A. Breeding strategy to generate Gγ8-tTA;tetO-hM4Di [Gγ8-hM4Di] experimental and tetO-hM4Di control mice. **B,C.** 60x

magnification maximum intensity projection confocal images of OE stained for DAPI (blue), HA (green), and GAP43 (magenta) in a Gγ8-hM4Di mouse (**B**) and a tetO-hM4Di mouse (**C**). Scale bar: 100 µm. **D.** Percentage of GAP43-positive OSNs that co-express the hM4Di receptor marked with the HA tag (Gγ8-hM4Di n = 5; tetO-hM4Di n = 3; Welch's t-test: $t(4) = 19.9$, $P < 0.001$). **E,F.** Example images of OBs from a saline-treated Gγ8-hM4Di mouse (**E**) and a CNO-treated Gγ8-hM4Di mouse (**F**) stained for PS6. Scale bars: 100 µm. **E',F'. G.** Linear density of PS6+ cells in the MCL is decreased by silencing immature OSN input (unpaired t-test: $t(6) = 2.54$, $P = 0.044$). **H,I.** Reduced PS6+ MC density when immature OSNs are silenced during odor exposure in dorsal (**H**) (unpaired t-test: $t(6) = 3.35$, $P = 0.015$) and ventral (**I**) (unpaired t-test: $t(6) = 2.46$, $P = 0.049$) MCL. **J.** Linear density of PS6+ cells in the MCL is not affected by CNO administration in tetO-hM4Di control mice (unpaired t-test: $t(3) = 0.81$, $P = 0.48$). **K, L.** No effect of CNO administration during odor exposure on linear density of PS6+ MCs in dorsal (**K**) (unpaired t-test: $t(3) = 0.65$, $P = 0.57$) or ventral (**L**) (unpaired t-test: $t(3) = 0.98$, $P = 0.40$) MCL in tetO-hM4Di control mice. Symbols: values for individual mice.

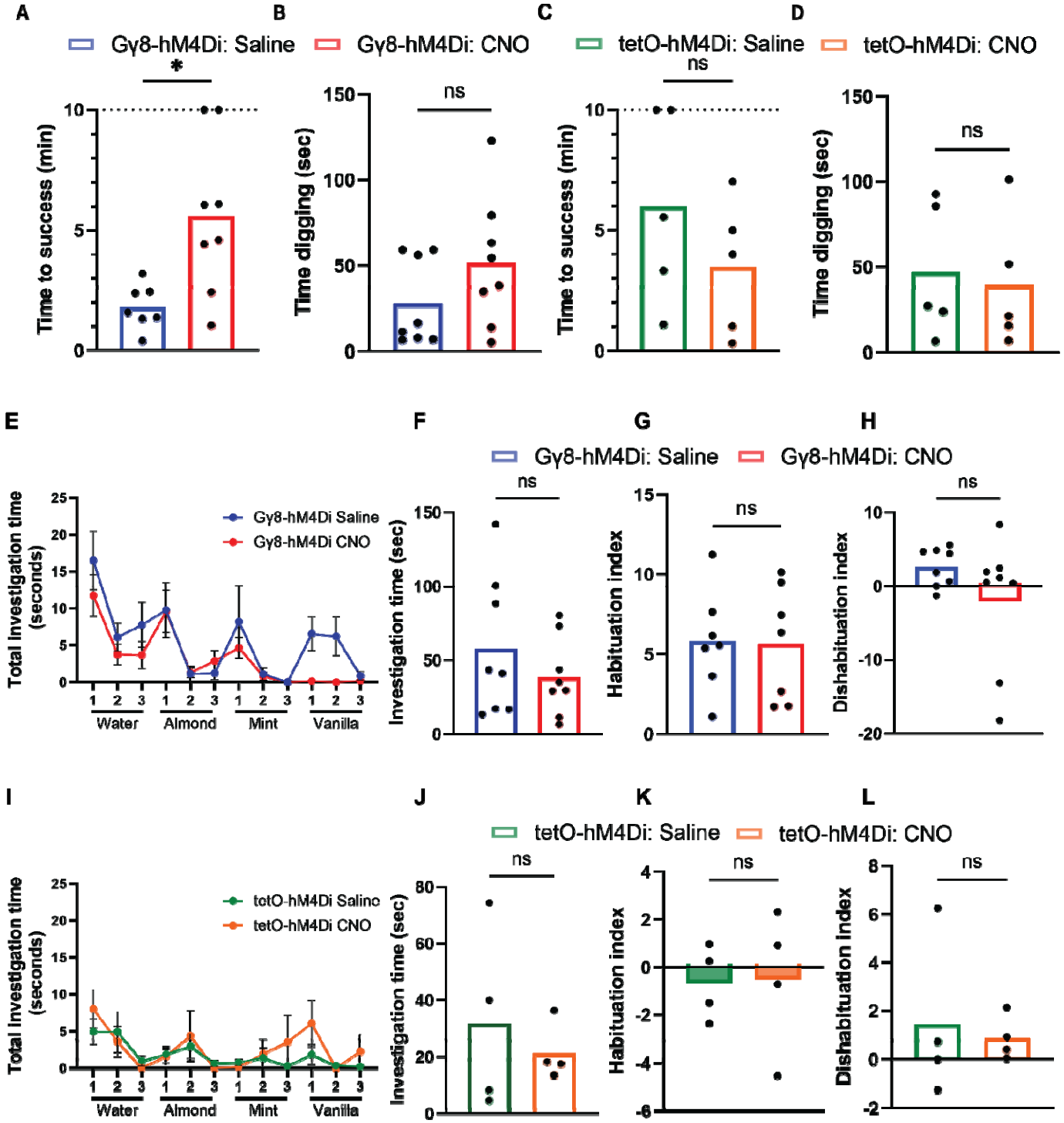

Figure 2. Immature OSNs contribute to odor detection, but not odor discrimination, abilities in the intact olfactory system. A. Silencing immature OSN input via CNO injection increases time to success in buried food task (unpaired t-test: $t(13) = 2.98$, $P = 0.011$, saline-treated Gγ8-hM4Di mice n = 7, CNO-treated Gγ8-hM4Di mice n = 8). Symbols: individual mice. **B.** Time spent digging in the buried food task did not differ between saline- and CNO-treated Gγ8-hM4Di mice (unpaired t-test: $t(14) = 1.47$, $P = 0.17$). Symbols: individual mice. **C.** CNO administration into tetO-hM4Di control mice does not affect odor detection abilities (unpaired t-test: $t(8) = 1.16$, $P = 0.28$, saline-treated tetO-hM4Di mice n = 5, CNO-treated tetO-hM4Di mice $n = 5$). Symbols: individual mice. **D.** Time spent digging in the buried food task did not differ between saline- and CNO-treated tetO-hM4Di mice

(unpaired t-test: t(8) = 0.32, P = 0.76). Symbols: individual mice. **E** Investigation time in an odor habituation-dishabituation assay for saline- and CNO-treated Gγ8-hM4Di (n = 8 per group). Symbols: mean. Bars: standard deviation. **F** Total investigation time during odor discrimination assay is not affected by CNO administration in Gγ8-hM4Di mice (unpaired t-test: t(14) = 1.00, P = 0.34). Symbols: individual mice. **G** Mean habituation index across odors is unaffected by CNO administration in Gγ8-hM4Di mice (unpaired t-test: t(12) = 0.088, P = 0.93). Symbols: individual mice. **H.** Mean dishabituation index is unaffected by CNO administration in Gγ8-hM4Di mice (unpaired t-test: t(14) = 1.43 , P = 0.18). Symbols: individual mice. **I.** Investigation time in an odor habituation-dishabituation assay for tetO-hM4Di mice (n = 4 per group). Symbols: mean. Bars: standard deviation. **J.** Total investigation time during odor discrimination assay is not affected by CNO administration in tetO-hM4Di control (unpaired t-test: t(6) = 0.62, P = 0.56). Symbols: individual mice. **K.** Mean habituation index across odors is unaffected by CNO administration in tetO-hM4Di mice (unpaired t-test: t(7) = 0.098, P = 0.93). Symbols: individual mice. **L.** Mean dishabituation index is unaffected by CNO administration in tetO-hM4Di mice (unpaired t-test: t(7) = 0.33, P = 0.76). Symbols: individual mice.

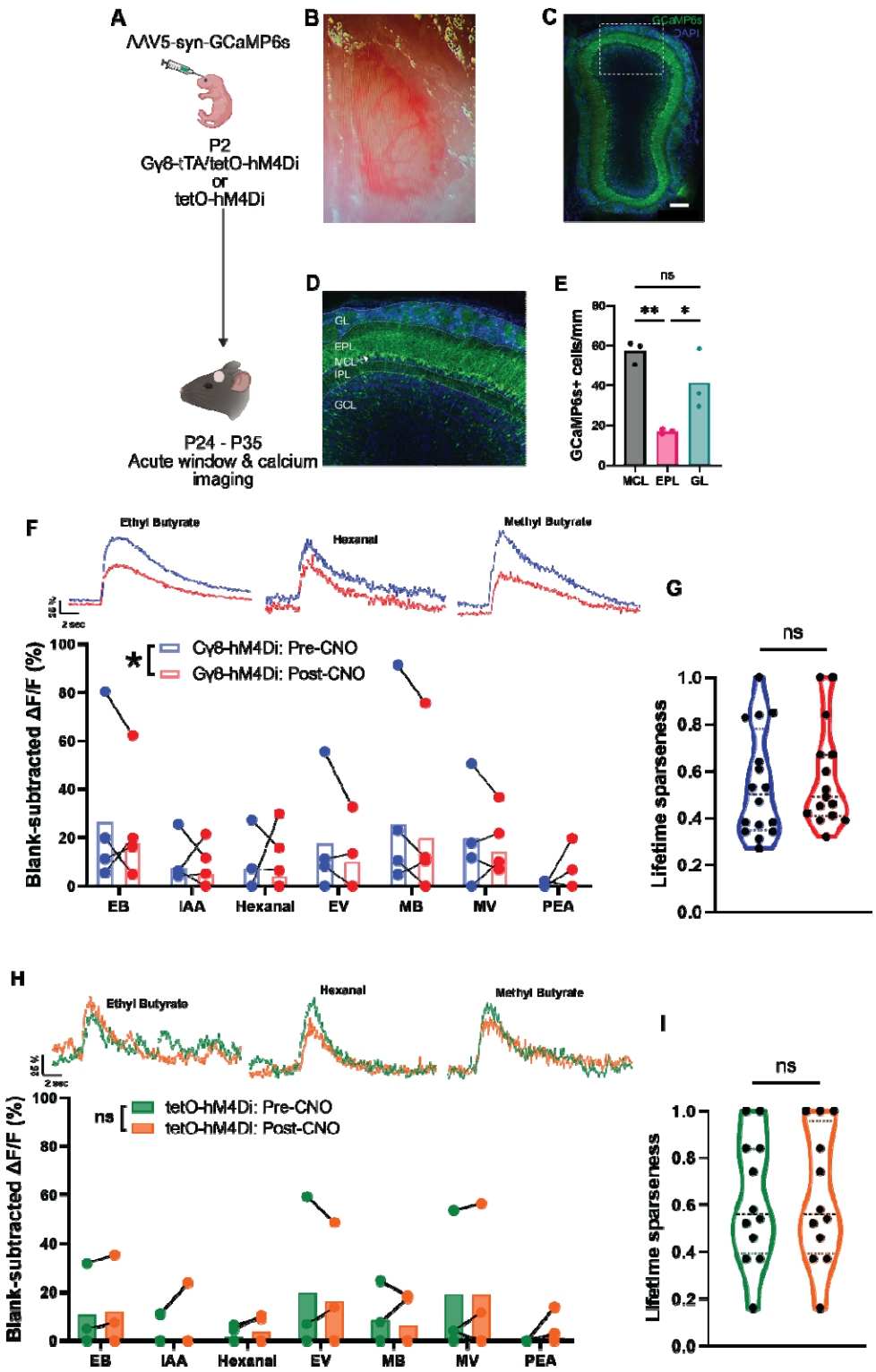

Figure 3. Acute silencing of immature OSN input dampens odor-evoked responses of postsynaptic cells across the OB. A. Neonatal injection strategy to introduce GCaMP6s into the OB for acute imaging. Gγ8-hM4Di (n = 4) and tetO-hM4Di (n = 4) mice received a 1 µL injection of AAV5-syn-GCaMP6s into the right OB at postnatal day 2 (P2). **B.** Acute cranial window placed over the right OB for 2-photon calcium imaging. **C.** Neonatal injection of AAV5-syn-GCaMP6s results in GCaMP6s expression that is stronger in the MCL and EPL. Stitched 10x magnification image of coronal OB showing GCaMP6s expression throughout the entire OB. Scale bar = 250 µm. **D.** Inset of

dorsal OB showing GCaMP6s expression is stronger in the MCL and EPL. IPL = internal plexiform layer, GCL = granule cell layer. **E.** Linear density of GCaMP6s+ cells in the MCL, EPL, and the GL shows a majority of GCaMP6s expressing cells are found in the MCL, suggesting that odor-evoked calcium responses recorded in the GL are likely comprised of MC and TC responses (One-way ANOVA, $P = 0.006$, $F_{2,6} = 13.7$. Tukey's multiple comparisons tests, MCL vs. EPL: $P = 0.004$. MCL vs. GL: $P = 0.19$. EPL vs. GL: $P = 0.045$. n = 3 mice). **F.** Acute silencing of immature OSNs via CNO injection decreases mean odor-evoked response amplitude in Gγ8-hM4Di mice (2-way ANOVA. Effect of CNO administration: $P = 0.014$, $F_{1,21} = 7.27$. Effect of odors: $P = 0.74$, $F_{1,21} = 0.58$. Interaction between odors and CNO administration: $P = 0.78$, $F_{1,21} = 0.53$. $n = 4$ mice). Odors used in panel: ethyl butyrate [EB], isoamyl acetate [IAA], hexanal [HEX], ethyl valerate [EV], methyl butyrate [MB], methyl valerate [MV], and phenethylamine [PEA]. Traces above graphs (from left to right) are example traces of EB-, HEX-, and MB-evoked responses before and after CNO administration. Symbols: individual mice. **G.** Lifetime sparseness of glomerular odorant responses is not affected by CNO administration in Gγ8-hM4Di mice (paired t-test. $P = 0.44$, $t(13) = 0.80$, n = 16 responding glomeruli from 4 mice). Symbols: values for individual glomeruli. **H.** CNO administration does not affect odor-evoked response amplitude in tetO-hM4Di control mice (2-way ANOVA. Effect of CNO: $P = 0.096$, $F_{1,21} = 3.04$. $n = 4$ mice. Effect of odors: $P = 0.80$, $F_{6,21} = 0.50$. Interaction between odors and CNO administration: $P = 0.91$, $F_{6,21} = 0.34$. $n = 4$ mice). Odors, traces and symbols as in (**F**). **I.** CNO does not affect lifetime sparseness of odor-evoked responses in tetO-hM4Di mice (paired t-test. $P = 0.34$, $t(10) = 1.00$. $n = 12$ responding glomeruli from 4 mice). Symbols: values for individual glomeruli.

References

1. Miragall, F., and Graziadei, G.M. (1982). Experimental studies on the olfactory marker protein. II. Appearance of the olfactory marker protein during differentiation of the olfactory sensory neurons of mouse: an immunohistochemical and autoradiographic study. Brain Res *239*, 245–250. https://doi.org/10.1016/0006-8993(82)90846-0.

2. Harding, J., Graziadei, P.P.C., Graziadei, G.A.M., and Margolis, F.L. (1977). Denervation in the primary olfactory pathway of mice. IV. Biochemical and morphological evidence for neuronal replacement following nerve section. Brain Res. *132*, 11–28. https://doi.org/10.1016/0006-8993(77)90703-x.

3. Huard, J.M.T., and Schwob, J.E. (1995). Cell cycle of globose basal cells in rat olfactory epithelium. Dev. Dyn. *203*, 17–26. https://doi.org/10.1002/aja.1002030103.

4. McIntyre, J.C., Titlow, W.B., and McClintock, T.S. (2010). Axon growth and guidance genes identify nascent, immature, and mature olfactory sensory neurons. Journal of Neuroscience Research *88*, 3243–3256. https://doi.org/10.1002/jnr.22497.

5. Verhaagen, J., Oestreicher, A., Gispen, W., and Margolis, F. (1989). The expression of the growth associated protein B50/GAP43 in the olfactory system of neonatal and adult rats. J. Neurosci. *9*, 683–691. https://doi.org/10.1523/jneurosci.09-02-00683.1989.

6. Schwob, J.E., Jang, W., Holbrook, E.H., Lin, B., Herrick, D.B., Peterson, J.N., and Coleman, J. (2017). Stem and progenitor cells of the mammalian olfactory epithelium: Taking poietic license. J Comp Neurol *525*, 1034–1054. https://doi.org/10.1002/cne.24105.

7. Nickell, M.D., Breheny, P., Stromberg, A.J., and McClintock, T.S. (2012). Genomics of mature and immature olfactory sensory neurons. J. Comp. Neurol. *520*, 2608–2629. https://doi.org/10.1002/cne.23052.

8. Ryba, N., and Tirindelli, R. (1995). A novel GTP-binding protein gamma-subunit, G gamma 8, is expressed during neurogenesis in the olfactory and vomeronasal neuroepithelia. J Biol Chem *270*, 6757–6767.

9. Tirindelli, R., and Ryba, N. (1996). The G-protein gamma-subunit G gamma 8 is expressed in the developing axons of olfactory and vomeronasal neurons. The European journal of neuroscience *8*, 2388–2398.

10. Rodriguez-Gil, D.J., Bartel, D.L., Jaspers, A.W., Mobley, A.S., Imamura, F., and Greer, C.A. (2015). Odorant receptors regulate the final glomerular coalescence of olfactory sensory neuron axons. Proc Natl Acad Sci *112*, 5821–5826. https://doi.org/10.1073/pnas.1417955112.

11. Holtmaat, A.J.G.D., Huizinga, C.T., Margolis, F.L., Gispen, W.H., and Verhaagen, J. (1999). Transgenic expression of B-50/GAP-43 in mature olfactory neurons triggers downregulation of native B-50/GAP-43 expression in immature olfactory neurons. Mol. Brain Res. *74*, 197–207. https://doi.org/10.1016/s0169-328x(99)00263-6.

12. Kondo, K., Suzukawa, K., Sakamoto, T., Watanabe, K., Kanaya, K., Ushio, M., Yamaguchi, T., Nibu, K., Kaga, K., and Yamasoba, T. (2010). Age-related changes in cell dynamics of the postnatal mouse olfactory neuroepithelium: Cell proliferation, neuronal differentiation, and cell death. J Comp Neurol *518*, 1962–1975. https://doi.org/10.1002/cne.22316.

13. Liberia, T., Martin-Lopez, E., Meller, S.J., and Greer, C.A. (2019). Sequential maturation of olfactory sensory neurons in the mature olfactory epithelium. Eneuro *6*, ENEURO.0266-19.2019. https://doi.org/10.1523/eneuro.0266-19.2019.

14. Savya, S.P., Kunkhyen, T., and Cheetham, C. (2019). Low survival rate of young adult-born olfactory sensory neurons in the undamaged mouse olfactory epithelium. J. Bioenerg. Biomembr. *51*, 41–51. https://doi.org/10.1007/s10863-018-9774-8.

15. Monahan, K., and Lomvardas, S. (2014). Monoallelic Expression of Olfactory Receptors. Annual Review of Cell and Developmental Biology *31*, 721–740. https://doi.org/10.1146/annurev-cellbio-100814-125308.

16. Mombaerts, P. (2004). Odorant receptor gene choice in olfactory sensory neurons: the one receptor–one neuron hypothesis revisited. Current Opinion in Neurobiology *14*, 31–36. https://doi.org/10.1016/j.conb.2004.01.014.

17. Vassar, R., Chao, S.K., Sitcheran, R., Nunez, J.M., Vosshall, L.B., and Axel, R. (1994). Topographic organization of sensory projections to the olfactory bulb. Cell *79*.

18. Serizawa, S., Ishii, T., Nakatani, H., Tsuboi, A., Nagawa, F., Asano, M., Sudo, K., Sakagami, J., Sakano, H., Ijiri, T., et al. (2000). Mutually exclusive expression of odorant receptor transgenes. Nat. Neurosci. *3*, 687–693. https://doi.org/10.1038/76641.

19. Shepherd, G.M. ed. (2004). The synaptic organization of the brain 5th ed.

20. McClintock, T.S., Khan, N., Xie, C., and Martens, J.R. (2020). Maturation of the Olfactory Sensory Neuron and Its Cilia. Chem. Senses *45*, 805–822. https://doi.org/10.1093/chemse/bjaa070.

21. Cheetham, C.E., Park, U., and Belluscio, L. (2016). Rapid and continuous activity-dependent plasticity of olfactory sensory input. Nature communications *7*, 10729. https://doi.org/10.1038/ncomms10729.

22. Marcucci, F., Maier-Balough, E., Zou, D., and Firestein, S. (2011). Exuberant growth and synapse formation of olfactory sensory neuron axonal arborizations. Journal of Comparative Neurology *519*, 3713–3726. https://doi.org/10.1002/cne.22684.

23. Huang, J.S., Kunkhyen, T., Rangel, A.N., Brechbill, T.R., Gregory, J.D., Winson-Bushby, E.D., Liu, B., Avon, J.T., Muggleton, R.J., and Cheetham, C.E.J. (2022). Immature olfactory sensory neurons provide behaviourally relevant sensory input to the olfactory bulb. Nat. Commun. *13*, 6194. https://doi.org/10.1038/s41467-022-33967-6.

24. Menco, B.P., and Farbman, A.I. (1985). Genesis of cilia and microvilli of rat nasal epithelia during pre-natal development: II. olfactory epithelium, a morphometric analysis. J. Cell Sci. *78*, 311–336. https://doi.org/10.1242/jcs.78.1.311.

25. Sakamoto, T., Kondo, K., Kashio, A., Suzukawa, K., and Yamasoba, T. (2007). Methimazole-induced cell death in rat olfactory receptor neurons occurs via apoptosis triggered through mitochondrial cytochrome c-mediated caspase-3 activation pathway. Journal of Neuroscience Research *85*, 548–557. https://doi.org/10.1002/jnr.21155.

26. Kunkhyen, T., Brechbill, T.R., Berg, S.P.R., Pothuri, P., Rangel, A.N., Gupta, A., and Cheetham, C.E.J. (2024). Cell type- and layer-specific plasticity of olfactory bulb interneurons following olfactory sensory neuron ablation. Sci. Rep. *14*, 17771. https://doi.org/10.1038/s41598-024-68649-4.

27. Salvi, S.S., Pati, S., Chaudhari, P.R., Tiwari, P., Banerjee, T., and Vaidya, V.A. (2019). Acute Chemogenetic Activation of CamKIIα-Positive Forebrain Excitatory Neurons Regulates Anxiety-Like Behaviour in Mice. Front Behav Neurosci *13*, 249. https://doi.org/10.3389/fnbeh.2019.00249.

28. Zhu, H., and Roth, B.L. (2014). Silencing Synapses with DREADDs. Neuron *82*, 723–725. https://doi.org/10.1016/j.neuron.2014.05.002.

29. Stachniak, T.J., Ghosh, A., and Sternson, S.M. (2014). Chemogenetic Synaptic Silencing of Neural Circuits Localizes a Hypothalamus→Midbrain Pathway for Feeding Behavior. Neuron *82*, 797–808. https://doi.org/10.1016/j.neuron.2014.04.008.

30. Nguyen, M.Q., Zhou, Z., Marks, C.A., Ryba, N.J.P., and Belluscio, L. (2007). Prominent Roles for Odorant Receptor Coding Sequences in Allelic Exclusion. Cell *131*, 1009–1017. https://doi.org/10.1016/j.cell.2007.10.050.

31. Gaun, V., Martens, J.R., and Schwob, J.E. (2022). Lifespan of mature olfactory sensory neurons varies with location in the mouse olfactory epithelium and age of the animal. J. Comp. Neurol. *530*, 2238–2251. https://doi.org/10.1002/cne.25330.

32. Hanchate, N.K., Kondoh, K., Lu, Z., Kuang, D., Ye, X., Qiu, X., Pachter, L., Trapnell, C., and Buck, L.B. (2015). Single-cell transcriptomics reveals receptor transformations during olfactory neurogenesis. Science *350*, 1251–1255. https://doi.org/10.1126/science.aad2456.

33. Tan, L., Li, Q., and Xie, S.X. (2015). Olfactory sensory neurons transiently express multiple olfactory receptors during development. Molecular Systems Biology *11*, 844. https://doi.org/10.15252/msb.20156639.

34. Duffié, R., Shayya, H., Arenal, M.E. del, Wang, M., Kahiapo, J., Ugurbil, A., Keskin, A., Clowney, F., Bashkirova, E.V., Pourmorady, A.D., et al. (2025). Mex3a-dependent post-transcriptional silencing ensures olfactory receptor diversity and axon guidance specificity. Cell Rep. *44*, 115979. https://doi.org/10.1016/j.celrep.2025.115979.

35. Kint, L.T., Seewoo, B.J., Hyndman, T.H., Clarke, M.W., Edwards, S.H., Rodger, J., Feindel, K.W., and Musk, G.C. (2020). The Pharmacokinetics of Medetomidine Administered Subcutaneously during Isoflurane Anaesthesia in Sprague-Dawley Rats. Animals *10*, 1050. https://doi.org/10.3390/ani10061050.

36. Adefuin, A.M., Lindeman, S., Reinert, J.K., and Fukunaga, I. (2022). State-dependent representations of mixtures by the olfactory bulb. eLife *11*, e76882. https://doi.org/10.7554/elife.76882.

37. Kollo, M., Schmaltz, A., Abdelhamid, M., Fukunaga, I., and Schaefer, A.T. (2014). “Silent” mitral cells dominate odor responses in the olfactory bulb of awake mice. Nat. Neurosci. *17*, 1313–1315. https://doi.org/10.1038/nn.3768.

38. Manvich, D.F., Webster, K.A., Foster, S.L., Farrell, M.S., Ritchie, J.C., Porter, J.H., and Weinshenker, D. (2018). The DREADD agonist clozapine N-oxide (CNO) is reverse-metabolized to clozapine and produces clozapine-like interoceptive stimulus effects in rats and mice. Sci. Rep. *8*, 3840. https://doi.org/10.1038/s41598-018-22116-z.

39. Jendryka, M., Palchaudhuri, M., Ursu, D., Veen, B. van der, Liss, B., Kätzel, D., Nissen, W., and Pekcec, A. (2019). Pharmacokinetic and pharmacodynamic actions of clozapine-N-oxide, clozapine, and compound 21 in DREADD-based chemogenetics in mice. Sci. Rep. *9*, 4522. https://doi.org/10.1038/s41598-019-41088-2.

40. Schindelin, J., Arganda-Carreras, I., Frise, E., Kaynig, V., Longair, M., Pietzsch, T., Preibisch, S., Rueden, C., Saalfeld, S., Schmid, B., et al. (2012). Fiji: an open-source platform for biological-image analysis. Nature Methods *9*, 676–682. https://doi.org/10.1038/nmeth.2019.

41. Yang, M., and Crawley, J.N. (2009). Simple Behavioral Assessment of Mouse Olfaction. Curr Protoc Neurosci *48*, 8.24.1-8.24.12. https://doi.org/10.1002/0471142301.ns0824s48.

42. Phifer, C.B., and Terry, L.M. (1986). Use of hypothermia for general anesthesia in preweanling rodents. Physiol. Behav. *38*, 887–890. https://doi.org/10.1016/0031-9384(86)90058-2.

43. Cheetham, C.E., Grier, B.D., and Belluscio, L. (2015). Bulk regional viral injection in neonatal mice enables structural and functional interrogation of defined neuronal populations throughout targeted brain areas. Frontiers in neural circuits *9*, 72. https://doi.org/10.3389/fncir.2015.00072.

44. Cheetham, C.E. (2018). Multiphoton intravital calcium imaging. Curr. Protoc. Cytom. *e40*, doi: 10.1002/cpcy.40.

Acknowledgements

Research reported in this manuscript was supported by the National Institute on Deafness and other Communication Disorders of the National Institutes of Health under Award Number R01DC018516 to C.E.J.C. The content is solely the responsibility of the authors and does not necessarily represent the official views of the National Institutes of Health. We thank members of the Cheetham lab for helpful discussions.

Declaration of Interests

The authors declare no competing interests.

Supplemental Material

Supplemental Figure

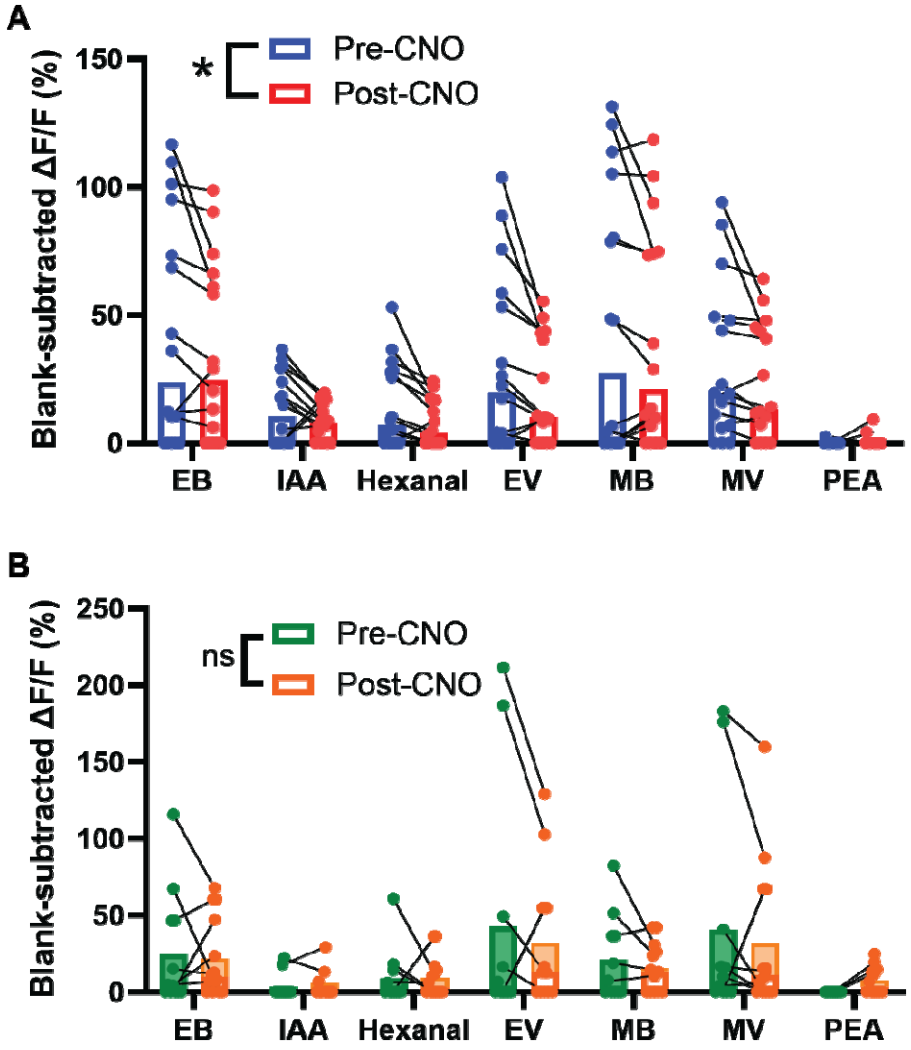

Figure S1. **Acute silencing of immature OSN input dampens odor-evoked responses of postsynaptic cells on a per-glomerulus basis. A**. Acute silencing of immature OSNs via CNO injection reduces mean odor-evoked responses in the individual glomeruli of Gγ8-hM4Di mice generally (2-way ANOVA. Effect of CNO administration: $P < 0.001$, $F_{1,105} = 22.8$. Effect on odors: $P < 0.001$, $F_{6,105} = 5.06$. Interaction between odors and CNO administration: $P = 0.34$, $F_{6,105} = 1.15$, n = 16 responsive glomeruli from 4 mice). **B**. CNO administration has no effect on odor-evoked responses in the glomeruli of tetO-hM4Di control mice generally (2-way ANOVA. Effect of CNO administration: $P = 0.43$, $F_{1,68} = 0.62$. Effect on odors: $P = 0.081$ $F_{6,86} = 1.96$. Interaction between odors and CNO administration: $P = 0.90$, $F_{6,68} = 0.37$, n = 14 responsive glomeruli from 4 mice). Odors used in panel: ethyl butyrate [EB], isoamyl acetate [IAA], hexanal [HEX], ethyl valerate [EV], methyl butyrate [MB], methyl valerate [MV], and phenethylamine [PEA].

Supplemental Video Legends

Supplemental Video 1. Glomerular layer odor-evoked responses in OB neuron dendrites. Representative video showing ethyl butyrate-evoked responses captured in the glomerular layer of the OB during odor presentation before CNO administration. Here, we see the emergence of ethyl butyrate responses in both dendritic processes throughout the glomeruli and surrounding cell bodies. Responses are shown in real time (15 frames per second).

Supplemental Video 2. Silencing immature OSNs reduces the amplitude of glomerular layer odor-evoked responses in OB neuron dendrites within glomeruli. Representative video of ethyl butyrate-evoked responses in the same field of view as in Supplemental Video 1 after CNO administration to silence immature OSNs. Odor-evoked responses in dendrites within the imaged glomeruli are reduced in amplitude relative to before CNO treatment.